Publ. Astron. Soc. Japan **39**, 457–473 (1987)

Global Trapped Oscillations of Relativistic Accretion Disks

Atsuo T. OKAZAKI

College of General Education, Hokkai-Gakuen University, Toyohira-ku, Sapporo 062

Shoji KATO

Department of Astronomy, University of Kyoto, Sakyo-ku, Kyoto 606

and

Jun FUKUE

Astronomical Institute, Osaka Kyoiku University, Tennoji-ku, Osaka 543

(Received 1986 January 10; accepted 1986 December 4)

Abstract

Axially symmetric, isothermal pulsations of a geometrically thin disk rotating around a nonrotating relativistic object are investigated. The disk is assumed to be isothermal in the vertical direction and to have a constant vertical scale height. It is found that there exist *global* pulsation modes trapped in an inner region of the disk. Eigenfrequencies of the modes are in the range of 0 to $\kappa_{\max}$, where $\kappa_{\max}$ is the maximum value of an epicyclic frequency in the disk. For an oscillation to be trapped in the disk, the eigenfunctions must have at least one node in the vertical direction. The trapping is related to the fact that, in relativistic disks, the radial distribution of the epicyclic frequency has a maximum at a certain radius. The results suggest that the presence of global trapped oscillation modes is a general characteristic of thin relativistic disks. The oscillation period obtained is briefly compared with observations.

Key words: Accretion disks; Active galactic nuclei; Compact stars; Pulsations; Trapped oscillations.

1. Introduction

It is well accepted that disk accretion onto a compact object is the machinery which generates tremendous energy in various astronomical objects such as active galactic nuclei, galactic X-ray sources, cataclysmic variables, and so on. Hence, observations of widely ranged periodic or quasi-periodic variabilities in many of these astronomical objects naturally lead astronomers to the idea that some of these variabilities are attributed to pulsations of accretion disks. Thus, oscillations of accretion disks have been investigated by many authors.

At present, however, the investigation appears to be limited mainly to geometrically thin, nonself-gravitating, nearly Keplerian disks because of their practical importance and of their simplicity. Even for such restricted disks, the work done so far is mainly on local oscillations [Van Horn et al. (1980); Cox (1981); Livio and Shaviv (1981); Cox and Everson (1983) for nearly vertical oscillations, and Kato (1978, 1979); Kato and Fukue (1980); Blumenthal et al. (1984) for nearly radial oscillations]. A general investigation of local oscillations (nonaxisymmetric oscillations with short wavelengths both in the vertical and in the horizontal directions) was done recently by Carroll et al. (1985).

Investigations of local oscillations are of importance to know the basic properties of disk oscillations. Local oscillations, however, cannot be the direct source of observed variabilities because incoherent oscillations at various places cannot produce a regular or semiregular large amplitude variation as a whole. Studies of global oscillations of disks are thus necessary in relation to observed variabilities. Such studies have been done little except by Kato (1983) and Okazaki and Kato (1985). In this paper, we examine global, isothermal oscillations of an isothermal relativistic Keplerian disk. The results show that there are axisymmetric global oscillation modes which are trapped in an inner region of the disk. These trapped oscillations will be common in relativistic disks as long as disks are geometrically thin. They are important observationally, because the inner region of the disks is the region where the most luminosity comes, and thus such oscillations will produce large amplitude variations.

The presence of trapped oscillations can be examined by considering how the propagation region of local waves is distributed in disks, as is done often in the study of nonradial oscillations of stars (e.g., Unno et al. 1979). Let us consider axisymmetric local oscillations with frequency ω. If the oscillations are mainly radial and have no nodes in the vertical direction, the wave propagation region in the radial direction is specified by $\omega > \kappa$, where κ is the epicyclic frequency. If the oscillations have node(s) in the vertical direction, however, a propagation region is changed to the region of $\omega < \kappa$. This will be mentioned later somewhat in detail.

In the latter case of $\omega < \kappa$, there is the possibility of the trapping of oscillations when the disks are relativistic. This is because, in the relativistic disks, the epicyclic frequency κ has a maximum $\kappa_{\max}$ at a certain radius near the inner edge of the disks (Kato and Fukue 1980), and decreases both inwards and outwards in the radial direction. Hence, around $\kappa_{\max}$ there is a limited region of $\omega < \kappa$. In this paper we shall demonstrate that the trapping of global oscillations around the radius of $\kappa = \kappa_{\max}$ really occurs, although the case considered is special.

In section 2 the unperturbed isothermal disk model is described and an isothermal perturbation is superposed on that disk. Then, a set of partial differential equations for a perturbed quantity is derived. When the disk's vertical scale height is constant in the radial direction, this set of equations is separated into ordinary differential equations. Section 3 gives the results on vertical oscillations. Section 4 discusses wave trapping in the radial direction, and the results on radial oscillations are given in section 5. The final section is devoted to discussion. The general relativistic epicyclic frequency is derived in the Appendix for the convenience of the reader.

2. Unperturbed Disk Model and Equations for Perturbations

2.1. *Unperturbed Disk Model*

As an unperturbed steady, axisymmetric disk, we consider a geometrically thin, nonself-gravitating perfect fluid rotating around a nonrotating compact object. The radius of the compact object is supposed to be less than $3r_g$, where r_g is the Schwarzschild radius specified by its mass M. It is assumed that the disk (with a constant molecular weight) is isothermal in the vertical direction but not so in the radial one. We adopt the cylindrical coordinates (r, ϕ, z) which are centered on the central object and have the z-axis in the direction perpendicular to the disk plane. General relativistic effects are simulated in terms of the so-called pseudo-Newtonian potential ψ defined by

$$\psi(r, z)=-\frac{GM}{(r^2+z^2)^{1/2}-r_g} \tag{2.1}$$

(e.g., Paczyński and Wiita 1980).

Since the disk is geometrically thin, the pressure force is negligible in the momentum balance in the radial direction, and the centrifugal force balances the gravitational one. Then it follows that the angular frequency $\Omega(r)$ of disk rotation is equal to the relativistic (strictly speaking, pseudo-Newtonian) Keplerian one $\Omega_K(r)$ defined by

$$\Omega_K(r)\equiv\left(\frac{1}{r}\frac{\partial\psi}{\partial r}\right)_{z=0}^{1/2}=\left[\frac{GM}{r(r-r_g)^2}\right]^{1/2}. \tag{2.2}$$

The equation describing the hydrostatic balance in the vertical direction is

$$\frac{1}{\rho_0}\frac{\partial p_0}{\partial z}=-\Omega_K{}^2 z\,. \tag{2.3}$$

Here ρ_0 and p_0 are the unperturbed density and pressure, respectively. Since the disk is isothermal in the vertical direction, equation (2.3) is easily integrated to give the density distribution in the vertical direction:

$$\rho_0(r, z)=\rho_{00}(r)\exp\left[-\frac{z^2}{2H^2(r)}\right]. \tag{2.4}$$

Here $\rho_{00}(r)$ is the unperturbed density on the equatorial plane and its functional form remains to be specified later. The scale height $H(r)$ of the disk is given by

$$H(r)=\frac{c_s(r)}{\Omega_K(r)}\,, \tag{2.5}$$

where $c_s(r)$ is the isothermal sound speed:

$$c_s(r)=\left(\frac{p_0}{\rho_0}\right)^{1/2}. \tag{2.6}$$

2.2. *Equations for Isothermal Perturbations*

A small-amplitude axisymmetric perturbation is superposed on the disk men-

tioned above. The perturbation is assumed to be isothermal:

$$p_1=c_s^2\rho_1\,, \tag{2.7}$$

where p_1 and ρ_1 are respectively the Eulerian perturbation of the pressure and that of the density. Although we adopt this assumption for mathematical simplicity, it is adequate for the case where the thermal time scale associated with the perturbation is less than the dynamical one.

The equation of continuity for the perturbation is

$$\frac{\partial\rho_1}{\partial t}+\frac{\partial}{r\partial r}(r\rho_0 u_r)+\frac{\partial}{\partial z}(\rho_0 u_z)=0\,, \tag{2.8}$$

and the equations of motion describing the perturbation are

$$\frac{\partial u_r}{\partial t}-2\Omega u_\phi=-\frac{1}{\rho_0}\frac{\partial p_1}{\partial r}+\frac{\rho_1}{\rho_0^2}\frac{\partial p_0}{\partial r}\,, \tag{2.9}$$

$$\frac{\partial u_\phi}{\partial t}+\frac{\kappa^2}{2\Omega}u_r=0\,, \tag{2.10}$$

$$\frac{\partial u_z}{\partial t}=-\frac{1}{\rho_0}\frac{\partial p_1}{\partial z}+\frac{\rho_1}{\rho_0^2}\frac{\partial p_0}{\partial z}\,, \tag{2.11}$$

where $\kappa(r)$ is the epicyclic frequency defined by

$$\kappa^2=2\Omega\left(2\Omega+r\frac{d\Omega}{dr}\right), \tag{2.12}$$

and (u_r, u_ϕ, u_z) is the velocity associated with the perturbation. Substituting equation (2.2) into equation (2.12), we find

$$\kappa=\left[\frac{GM(r-3r_g)}{r(r-r_g)^3}\right]^{1/2}. \tag{2.13}$$

Note that the epicyclic frequency has its maximum $[(\sqrt{3}-1)/(2+\sqrt{3})(1+\sqrt{3})^3]^{1/2}\times(GM/r_g^3)^{1/2}$ at $r=(2+\sqrt{3})r_g$ in this pseudo-Newtonian treatment, while it does at $r=4r_g$ in the relativistic one [see equation (4.1) of Kato and Fukue (1980) or equation (A16) of this paper].

We seek for solutions which vary as $\exp(i\omega t)$, where ω is the frequency of the perturbation. Eliminating u_ϕ and u_z from equations (2.8)–(2.11) after replacing $\partial/\partial t$ by $i\omega$, we have a set of partial differential equations for $u_r(r, z)$ and $h_1(r, z)$:

$$\frac{\partial u_r}{\partial r}+\frac{d\ln r\rho_{00}}{dr}u_r=-\frac{i}{\omega}\left(\frac{\partial^2 h_1}{\partial z^2}-\frac{z}{H^2}\frac{\partial h_1}{\partial z}+\frac{\omega^2}{c_s^2}h_1\right), \tag{2.14}$$

$$\frac{\partial h_1}{\partial r}-\frac{d\ln T_0}{dr}h_1=-\frac{i}{\omega}(\omega^2-\kappa^2)u_r\,, \tag{2.15}$$

where h_1 is defined as

$$h_1(r, z)=\frac{p_1}{\rho_0}\,. \tag{2.16}$$

Here we have used the assumption that the disk temperature T_0 is independent of z, and also the relation $\partial \ln \rho_0/\partial z=-z/H^2$ which comes from equation (2.4).

It is difficult to solve a set of equations (2.14) and (2.15) in general. Hence, as the first step, we restrict our consideration to the mathematically simplest case where the scale height H is constant in the radial direction. Note that in this case the temperature varies as

$$T_0\propto r^{-1}(r-r_g)^{-2}\,. \tag{2.17}$$

The solution of equations (2.14) and (2.15) then can be written in separable forms:

$$\begin{aligned} u_r(r, z)&=i\omega y(r)g(z)\,,\\ h_1(r, z)&=f(r)g(z)\,. \end{aligned} \tag{2.18}$$

Substitution of equations (2.18) into equations (2.14) and (2.15) gives a set of the first-order ordinary differential equations for $y(r)$ and $f(r)$:

$$\frac{dy}{dr}=-\frac{d\ln r\rho_{00}}{dr}y-\frac{1}{\omega^2 c_s{}^2}(\omega^2-K\Omega_K{}^2)f\,, \tag{2.19}$$

$$\frac{df}{dr}=(\omega^2-\kappa^2)y+\frac{d\ln T_0}{dr}f\,, \tag{2.20}$$

and the second-order ordinary differential equation for $g(z)$:

$$H^2\frac{d^2g}{dz^2}-z\frac{dg}{dz}+Kg=0\,, \tag{2.21}$$

where K is a constant. The value of K is determined, with relevant boundary conditions, as the eigenvalue of equation (2.21). The basic equations to be solved in this paper are thus equations (2.19)–(2.21).

3. Vertical Component of Isothermal Pulsations

Equation (2.21) is solved first to find the vertical component of oscillations, $g(z)$, and the eigenvalue K. To do so, we introduce the dimensionless vertical coordinate ξ defined by

$$\xi=\frac{z}{H}\,. \tag{3.1}$$

Equation (2.21) is then reduced to

$$\frac{d^2g(\xi)}{d\xi^2}-\xi\frac{dg(\xi)}{d\xi}+Kg(\xi)=0\,. \tag{3.2}$$

Boundary conditions for equation (3.2) are taken on the equatorial plane ($\xi=0$) and at great distances ($|\xi| \to \infty$).

We distinguish oscillations by the parity of their vertical components. Hence, the condition on the equatorial plane is

$$\left.\begin{array}{ll} g=0 & \text{(odd mode)} \\ \dfrac{dg}{d\xi}=0 & \text{(even mode)} \end{array}\right\} \quad \text{at } \xi=0\,, \tag{3.3}$$

or

where even (odd) modes denote those whose vertical components of oscillations are symmetric (antisymmetric) with respect to the equatorial plane.

Next, we shall discuss the boundary condition to be posed at great distances. The proper condition at large $|\xi|$ is that the energy density for perturbations is bound, i.e., all quantities such as $\rho_0 u_r^2$, $\rho_0 u_z^2$, and p_1 are bound at great distances. Inspecting equations (2.9) to (2.11) and equation (2.16), we see that the above condition is satisfied if and only if $\rho_0^{1/2} h_1$ is bound at sufficiently large $|\xi|$. Hence, by use of equations (2.4), (2.18), and (3.1), the relevant boundary condition at great distances is finally reduced to

$$\exp(-\xi^2/4) g(\xi) \text{ is bound in the asymptotic region } |\xi| \to \infty\,. \tag{3.4}$$

Solutions we are interested in are those which satisfy conditions (3.3) and (3.4) and are regular everywhere at finite ξ. Thus, we find a solution for $g(\xi)$ in the form:

$$g(\xi)=\xi^s(a_0+a_2\xi^2+\cdots+a_{2n}\xi^{2n}+\cdots)\,, \tag{3.5}$$

where $a_0 \neq 0$ and $s \geqq 0$.

Equation (3.2) is to be valid for all values of ξ, so that when the series (3.5) is substituted into equation (3.2), the coefficient of each power of ξ can be equated to zero.

$$\begin{gathered} s(s-1)a_0=0\,, \\ (s+2n+2)(s+2n+1)a_{2n+2}-(s+2n-K)a_{2n}=0 \quad (n=0, 1, 2, \cdots)\,. \end{gathered} \tag{3.6}$$

Since $a_0 \neq 0$, the first of the recurrence relation (3.6) tells that $s=0$ or $s=1$. Hence, the series (3.5) denotes an even or an odd mode, corresponding to $s=0$ or $s=1$, respectively. It should be noted that the boundary condition (3.3) is automatically satisfied.

It follows from the second of the relation (3.6) that the presence of a finite or an infinite number of terms in series (3.5) depends on the choice of K. If the series does not terminate, its dominant asymptotic behavior can be inferred from the coefficients of its high terms:

$$\frac{a_{2n+2}}{a_{2n}} \to \frac{1}{2n} \quad \text{as } n \to \infty\,. \tag{3.7}$$

This ratio is the same as that of the series for $\xi^m \exp(\xi^2/2)$ with any finite value of m. Consequently, it is obvious that this behavior for $g(\xi)$ violates the boundary condition (3.4).

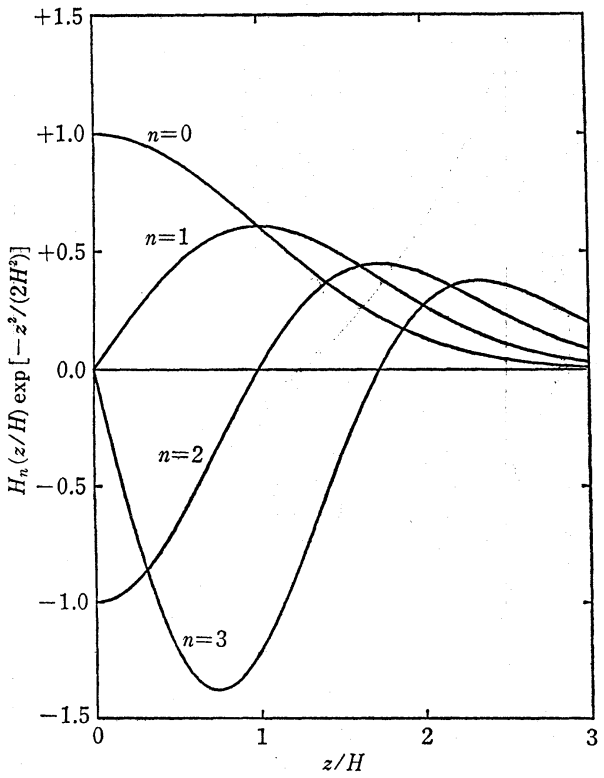

Fig. 1. Functional form of $g(\xi)\exp(-\xi^2/2)$ for the lowest four eigenmodes in the vertical direction.

Therefore, series (3.5) must terminate. This means

$$K=2m+s\,, \tag{3.8}$$

where m is a non-negative integer and the value of s is either zero or unity. We may express this equation in terms of a number n:

$$K=n \quad (n=0, 1, 2, \cdots)\,. \tag{3.9}$$

Equation (3.2) becomes then

$$\frac{d^2g(\xi)}{d\xi^2}-\xi\frac{dg(\xi)}{d\xi}+ng(\xi)=0 \quad (n=0, 1, 2, \cdots)\,. \tag{3.10}$$

Here an even (odd) n corresponds to an even (odd) mode of oscillation.

As is well known, a solution of equation (3.10) is the Hermite polynomial of order n. Hence, we may put $g(\xi)$ as

$$g(\xi)=H_n(\xi) \quad (n=0, 1, 2, \cdots)\,, \tag{3.11}$$

because the normalization constant is arbitrary now. The functional form of $g(\xi)\exp(-\xi^2/2)$ is shown in figure 1 with $n=0$ to 3.

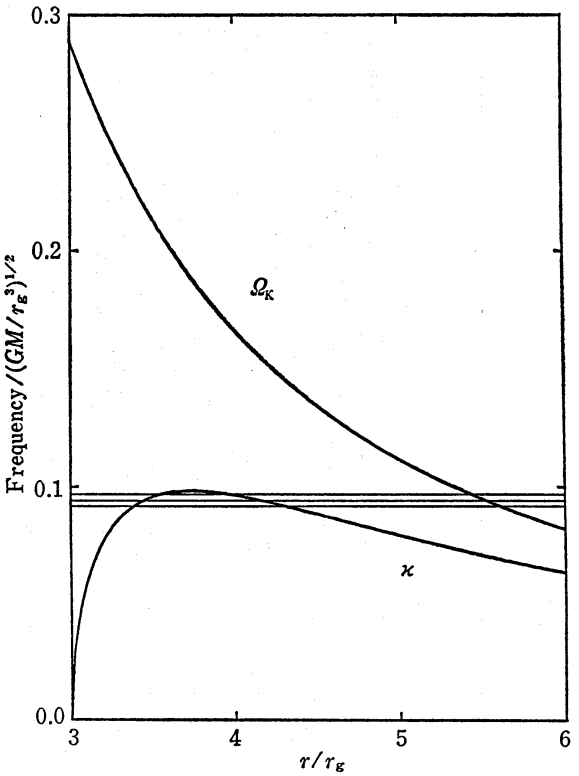

Fig. 2. Keplerian angular frequency Ω_K and epicyclic frequency κ in the pseudo-Newtonian potential as a function of r. The upper thick curve represents Ω_K and the lower one κ. Note that κ has the maximum $[(\sqrt{3}-1)/(2+\sqrt{3})(1+\sqrt{3})^3]^{1/2}(GM/r_g^3)^{1/2}$ at $r=(2+\sqrt{3})r_g$. The thin horizontal lines show values of eigenfrequency ω for the three lowest modes with $n=1$ under $H/r_g=3\times10^{-2}$ and $\rho_{00}=$constant. They correspond to (0, 1), (1, 1), and (2, 1) modes from top to bottom.

4. Wave Trapping in the Radial Direction

Before solving the set of equations (2.19) and (2.20) with $K=n$, we examine what oscillations are trapped in the radial direction as standing waves. For this purpose, it is convenient to rewrite equations (2.19) and (2.20) into canonical forms:

$$\frac{dY}{dr}=-\frac{1}{\omega^2 c_s^2}(\omega^2-n\Omega_K^2)r\rho_{00}T_0F\,, \tag{4.1}$$

$$\frac{dF}{dr}=(\omega^2-\kappa^2)(r\rho_{00}T_0)^{-1}Y\,, \tag{4.2}$$

where

$$Y=r\rho_{00}y \text{ and } F=f/T_0\,. \tag{4.3}$$

Qualitative features of the oscillations can be obtained by the local treatment, in which the r-dependence of coefficients in equations (4.1) and (4.2) is neglected. After taking Y and F to be proportional to exp (ikr), we have the *dispersion relation* for the present problem:

$$k^2=\frac{(\omega^2-\kappa^2)(\omega^2-n\Omega_K{}^2)}{\omega^2 c_s{}^2}\,. \tag{4.4}$$

Equation (4.4) shows that local waves with $n=0$ (no node in the vertical direction) can propagate in regions where $\omega>\kappa$ and must evanesce in the other regions. On the other hand, local waves with $n\neq 0$ can propagate in regions where $\omega<\kappa$ or $\omega>n^{1/2}\Omega_K$ and must evanesce in the other regions. To visualize the propagation region definitely, the radial dependence of two kinds of frequencies, Ω_K and κ, is shown in figure 2 by thick curves. As was noted in section 1, the epicyclic frequency κ in relativistic disks does not monotonically increase with decreasing r. It arrives at the maximum κ_{max} at $r=(2+\sqrt{3})r_g$ (in the pseudo-Newtonian potential), and vanishes at $r=3r_g$.

From figure 2 we see that local waves with $n=0$ can propagate everywhere in the disk when $\omega>\kappa_{max}$, while they can propagate inside LR_1 or outside LR_2 when $\omega<\kappa_{max}$ (cf. Kato and Fukue 1980). Here LR_1 and LR_2 are radii where $\omega=\kappa$ and defined so that $LR_1<LR_2$. On the other hand, *waves with $n\neq 0$ can propagate in a bound region between LR_1 and LR_2 when $\omega\leqq\kappa_{max}$*, although they penetrate partially into the outer propagation region of $\omega>n^{1/2}\Omega_K$.

The above consideration on the propagation region of local waves suggests that when $n\neq 0$, there will exist global oscillation modes trapped in the region between LR_1 and LR_2. In the next section we shall show this by numerical calculations.

5. Numerical Results on Radial Pulsation

In this section we solve equations (2.19) and (2.20) with relevant boundary conditions. Since our main attention is on the oscillations which are trapped in the region around $\kappa=\kappa_{max}$, the boundary conditions to be adopted are that the wave amplitude is negligible both near the inner edge of the disk ($r=3r_g$) and at radii far outside LR_2. In our present problem, however, a wave propagation region of $\omega>n^{1/2}\Omega_K$ appears a little outside of LR_2, as discussed in the previous section and seen from figure 2. Hence, as the outer boundary condition, we take here that the wave amplitude is negligible at a radius r_{out} just inside this outer propagation region. The boundary conditions adopted are thus

$$f(r)=0 \quad \text{at } r=3r_g \text{ and } r=r_{out}\,. \tag{5.1}$$

The radius r_{out} cannot be specified before solving equations (2.19) and (2.20); it is obtained simultaneously with ω, because r_{out} depends on the value of ω.

If the amplitude of oscillations obtained by use of the above boundary conditions is sufficiently small at $r\gtrsim 3r_g$ and $r\lesssim r_{out}$, the oscillations are well trapped and boundary conditions (5.1) are relevant. Otherwise, the adoption of boundary conditions (5.1) is too artificial, because in real situations the oscillations penetrate away into the surrounding propagation region. In other words, trapping is incomplete. Final numerical results, however, show that the wave trapping is rather complete in the case when the disk is thin. A brief discussion on the validity of the boundary conditions (5.1) will be presented in the last section.

In the following we classify each eigenmode by the numbers of nodes of eigen-

Table 1. Effects of the density profile on eigenfrequencies.

$\frac{d\ln\rho_{00}}{d\ln r}$	ω*		
	(0, 1)	(1, 1)	(2, 1)
+5	9.666 (−2)†	9.400 (−2)	9.154 (−2)
0	9.664 (−2)	9.400 (−2)	9.153 (−2)
−5	9.659 (−2)	9.394 (−2)	9.148 (−2)

* Eigenfrequencies are measured in units of $(GM/r_g^3)^{1/2}$. $H/r_g=3\times10^{-2}$ is assumed.

† The number in parentheses denotes a power of ten.

functions $y(r)$ and $g(\xi)$. For example, the (m, n) mode represents the one which has m node(s) in the radial direction and n node(s) in the vertical direction $(-\infty<\xi<+\infty)$. Since $g(\xi)$ is an Hermite polynomial, even (or odd) n denotes the mode whose eigenfunction is symmetric (or antisymmetric) with respect to the equatorial plane. When we refer to the eigenfrequency ω of the (m, n) mode in particular, we write it as $\omega(m, n)$.

It is noted here that parameters which will appear when equations (2.19) and (2.20) are changed into dimensionless forms are $d\ln\rho_{00}/d\ln r$ and H/r_g.

In figure 2 the thin horizontal lines show the values of eigenfrequency ω for the three lowest eigenmodes with $n=1$ under $H/r_g=3\times10^{-2}$ and $\rho_{00}=$constant. They are for (0, 1), (1, 1), and (2, 1) modes from top to bottom. It is readily observed that the value of ω decreases with increase of the node number in the radial direction. As is supposed from the form of equation (4.4), the results are less sensitive on the functional form of $\rho_{00}(r)$. Table 1 shows this; differences among results for $d\ln\rho_{00}/d\ln r=+5$, 0, and -5 are very small. Hence, we consider only the case of $\rho_{00}=$constant for the rest of this paper.

Figure 3 shows radial dependence of eigenfunctions $y(r)$ and $f(r)$ and the corresponding $k^2(r)$ profile with $H/r_g=3\times10^{-2}$ and $\rho_{00}=$constant. Figures 3a, 3b, and 3c are for (0, 1), (1, 1), and (2, 1) modes, respectively. In the upper part of each figure, $y(r)$ and $f(r)$ are respectively shown by solid and dashed curves, while in the lower part $k^2(r)r_g^2$. Short vertical lines crossing the horizontal axis denote the radii LR_1 and LR_2, which are, in a rough sense, good indicators of the radial extent of the oscillations. Also shown in each lower figure is the value of I defined by

$$I=\int_{LR_1}^{LR_2}k(r)dr\,. \tag{5.2}$$

The integral value I is helpful to compare numerical results with those obtained by the WKBJ method. This comparison will be made in the next section.

Figure 3 also shows that the radial extent of the lower mode is narrower than that of the higher one. In other words, the width of trapped regions becomes narrower with increasing ω.

Figure 4 shows the eigenfrequency ω as a function of H/r_g for some modes. A label attached to each line denotes the mode. Solid lines are for $(m, 1)$ modes and broken lines are for $(m, 2)$ modes with $m=0$ to 2. This figure shows that the value of $\omega(m, n)$ for given m and n gradually increases and approaches $\kappa_{\max}$ with decreasing H. It is also shown that the value of $\omega(m, n)$ increases with decreasing m or with increasing n.

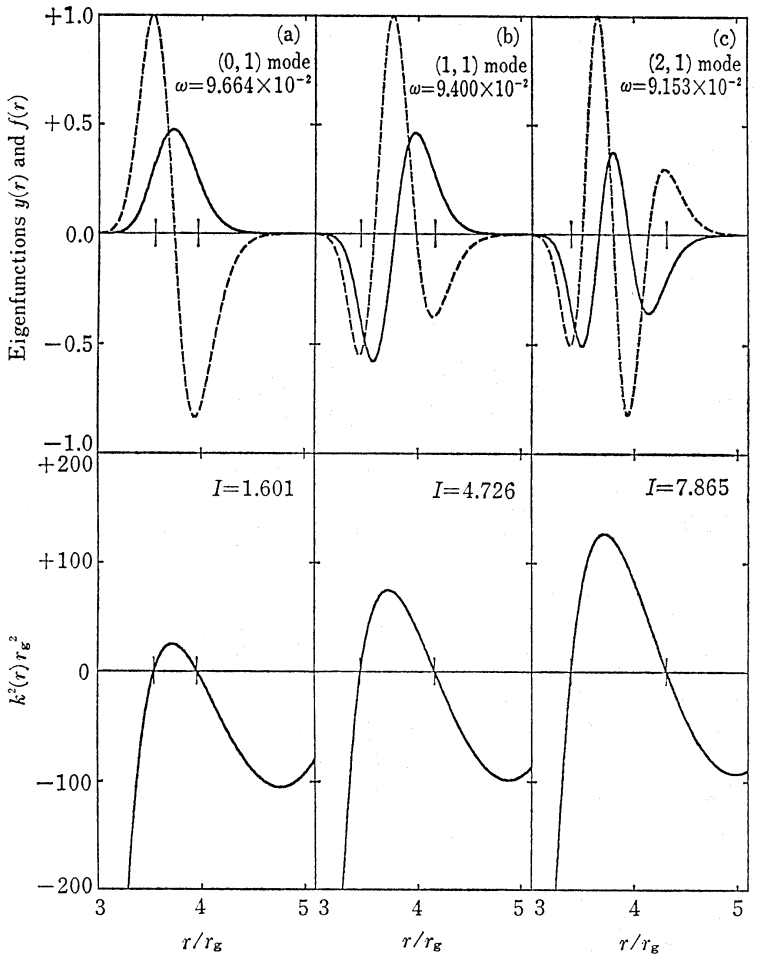

Fig. 3. Radial eigenfunctions, $y(r)$ and $f(r)$, and corresponding $k^2(r)$ profile for the three eigenmodes shown in figure 2: (a) the (0, 1) mode, (b) the (1, 1) mode, and (c) the (2, 1) mode. Eigenfunctions $y(r)$ and $f(r)$ are respectively denoted by solid curves and dashed ones in the upper panel while $k^2r_g^2$ is in the lower one. In the upper panel, the curves are normalized so that the maximum value of $f(r)$ is unity, Units of $y(r)$ are $50/(H/r_g)^2$ for (0, 1) mode and $20/(H/r_g)^2$ for (1, 1) and (2, 1) modes. In each figure, short vertical lines crossing the horizontal axis represent LR_1 and LR_2, the radii of $\omega=\kappa$. The eigenfrequency ω is written in the upper panel in units of $(GM/r_g^3)^{1/2}$. Also written in the lower panel is the value of integral I.

6. Discussion

We have shown that trapped modes of isothermal global oscillations are present in an inner part of a relativistic thin disk. The disk adopted is isothermal in the vertical direction and its vertical scale height is constant in the radial direction. For oscillations to be trapped, they must have nodes in the vertical direction. Their frequencies are in the range of 0 to $\kappa_{\max}$ (see figure 2).

The trapping comes from the facts that (i) the region of $\omega<\kappa$ is a propagation region of local waves of ω when $n\neq 0$, and (ii) in relativistic disks the epicyclic frequency κ has a maximum and thus the region of $\omega\leqq\kappa$ is bound when $\omega<\kappa_{\max}$. The former,

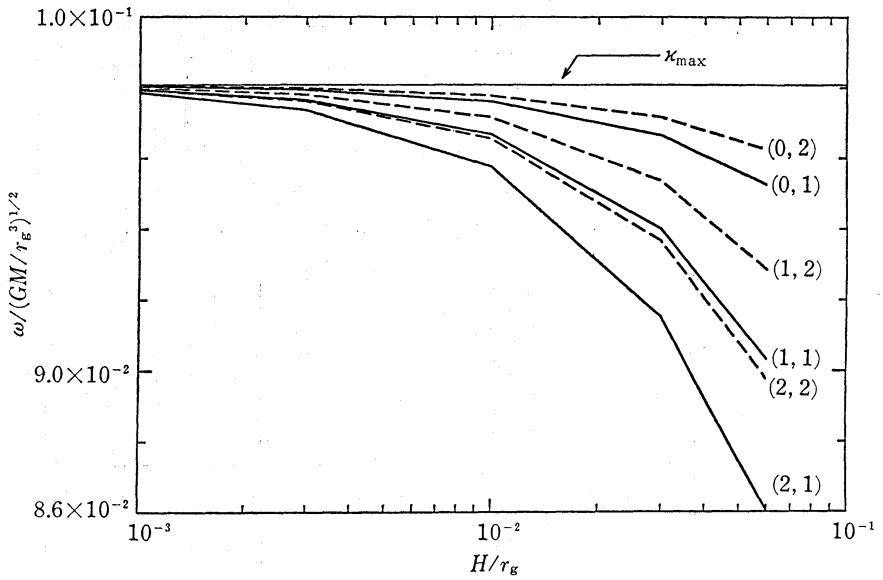

Fig. 4. Eigenfrequency ω as a function of the scale-height H. A label characterizing the mode is attached to each line.

i.e., (i), is a result of the local dispersion relation (4.4), and is free from the global structure of disks. The latter, i.e., (ii), is also a general characteristic of thin relativistic disks. Hence we consider that the presence of trapped wave modes is free from the detailed disk structure, and is a common feature of thin relativistic disks.

First we shall discuss the validity of the boundary conditions adopted. We have limited our attention to the case of thin disks with $H/r_g<10^{-1}$. This is because boundary conditions (5.1) are relevant only in such thin cases. If the disk is thicker (the pressure is higher), the trapping of waves is incomplete for the two following reasons. With increasing disk thickness, the eigenfrequency of (trapped) oscillations decreases and thus the radial width of the surrounding evanescent regions becomes narrower (see figure 2). Second, the damping rate of wave amplitude in the evanescent region becomes lower (notice that $|k^2|$ becomes smaller when the disk is thicker). Because of these two situations, the boundary conditions that the wave amplitude vanishes at $r=3r_g$ and $r=r_{out}$ are found to be irrelevant when the disk is thick. In particular, the inner boundary condition imposed at $r=3r_g$ seems to be so when H/r_g is larger than 0.1. (As will be seen below, the outer boundary condition is still relevant for disks with $H/r_g\sim0.1$.) In other words, when the disk is thick, more elaborate boundary conditions such as radiation conditions should be adopted. In such cases, the trapping is incomplete and oscillations will become damping ones. Examination of these cases is beyond the scope of this paper.

Next we compare our results with those derived from the WKBJ method, which has been used extensively in the field of nonradial oscillations of stars to find the asymptotic solutions of eigenvalues and eigenfunctions.

If the leakage of waves into surrounding regions is taken into account, the frequency ω becomes complex as $\omega=\omega_r+i\omega_i$ with $\omega_i/\omega_r\ll1$, ω_r and ω_i being the real part and the imaginary part of ω, respectively. Then equation (4.4) shows that the

radial wavenumber $k(r)$ in the region between LR_1 and LR_2 is written approximately as

$$k(r)=k_r+ik_i\cong\frac{(\kappa^2-\omega_r^2)^{1/2}(n\Omega_K^2-\omega_r^2)^{1/2}}{\omega_r\Omega_K H}\left(1-i\frac{\omega_r^2}{\kappa^2-\omega_r^2}\frac{\omega_i}{\omega_r}\right), \tag{6.1}$$

where $\kappa^2-\omega_r^2\ll\kappa^2$, ω_r^2 has been used. According to the WKBJ method (Shibahashi 1979; Unno et al. 1979), the eigenvalue condition is then given by

$$\int_{LR_1}^{LR_2}k_r(r)dr=(m+1/2)\pi \qquad (m=0, 1, 2, \cdots). \tag{6.2}$$

The damping rate ω_i of the oscillations due to leakage into the region of $\omega_r>n^{1/2}\Omega_K$ is estimated from

$$\tanh\left(\int_{LR_1}^{LR_2}k_i dr\right)\cong-\frac{1}{4}\exp\left(-2\int_{LR_2}^{r_0}|k|dr\right) \tag{6.3}$$

as

$$\frac{\omega_i}{\omega_r}\cong\frac{1}{4}\left(\frac{H}{r_g}\right)^2\left(\int_{LR_1}^{LR_2}\frac{n\Omega_K^2-\kappa^2}{\Omega_K^2}\frac{dr}{k_r r_g^2}\right)^{-1}\exp\left(-2\int_{LR_2}^{r_0}|k|dr\right)$$
$$\ll\exp\left(-2\int_{LR_2}^{r_0}|k|dr\right). \tag{6.4}$$

Here r_0 is the radius where $\omega_r=n^{1/2}\Omega_K$. In deriving equation (6.4) from equation (6.3), equation (6.1) has been used.

Comparison of condition (6.2) with the integral I given by equation (5.2) shows that the WKBJ method is accurate enough to find the eigenvalue in our present problem.

The value of $|k|$ vanishes near $r=LR_2$ and $r=r_0$, and between them it has the maximum value which is smaller than $n^{1/2}/H$. If $|k|=n^{1/2}/2H$ is substituted into equation (6.4), we have

$$\frac{\omega_i}{\omega_r}\ll\exp\left(-n^{1/2}\frac{l}{H}\right), \tag{6.5}$$

where $l=r_0-LR_2$. In the case of $H/r_g=3\times10^{-2}$ and $n=1$, we have $l\sim1.5r_g$ and the exponential term becomes $\sim\exp(-50)$. This implies that the leakage of waves into the region of $r>r_0$ is practically negligible, as is already known by numerical calculations.

We should mention here briefly some intrinsic differences between the results obtained in this paper and those in local vertical pulsations. The latter is for one dimensional (i.e., vertical) local oscillations. An ensemble of local incoherent oscillations with Keplerian periods results in a continuous spectrum in periods. On the other hand, the former is for two dimensional global oscillations. The inner part of the disk pulsates coherently with a time scale determined only by the mass of the central object.

Now, we discuss the observational appearance. When an optically thick disk

pulsates isothermally, there is no variation in disk luminosity. (Pulsations of disks studied in this paper vary the disk luminosity only when the disks are optically thin and the rotation axes of the disks are oblique to the line-of-sight direction.) Isothermal pulsations, however, have been considered only to show a concrete example of trapped oscillations. The presence of trapped oscillations will not be limited only to isothermal disks as mentioned before. In general cases time variations of disk luminosity will occur by pulsations. Furthermore, since the pulsating region is the inner part of disks, which is the most luminous region of disks, pulsations will effectively produce much change in the total luminosity.

The pulsation period P is

$$P=8.75\times10^{-4}\left[\frac{\omega}{0.1(GM/r_g^3)^{1/2}}\right]^{-1}\left(\frac{M}{M_\odot}\right)\mathrm{s}\,. \tag{6.6}$$

Periods of low modes are, roughly speaking, 1 ms for neutron stars and 1 d for $10^8 M_\odot$ black holes because $\omega\sim\kappa_{\max}\sim0.1(GM/r_g^3)^{1/2}$. In this paper our attention was only on the case when the central object is nonrotating. However, the results that there are trapped oscillation modes with $\omega\sim\kappa_{\max}$ will be extended to the case when the central object is rotating, because the circumstances leading to their presence (see the second paragraph in this section) are unchanged. When the central object is rotating, the frequency of trapped oscillations will become higher in comparison with that in the case of no rotation, because $\kappa_{\max}$ is higher in the rotating case than in the nonrotating one. In the Appendix the radial dependence of κ in general relativity is derived. Equation (A16) shows that the general relativistic $\kappa_{\max}$ observed at infinity ranges from 1/16 (Schwarzschild black holes) to ~0.2 (extreme Kerr holes) in units of $(GM/r_g^3)^{1/2}$.

Cyg X-1, a black hole of $\sim10\,M_\odot$, exhibits rapid X-ray variability whose time scale covers a range from milliseconds to seconds (e.g., Liang and Nolan 1984). Although the variability is chaotic, the power spectrum of the variability shows that there is a peak at a time scale somewhat smaller than 10 ms (Meekins et al. 1984). This time scale is consistent with pulsation periods provided that the central black hole rotates rapidly. Moreover, we know that several active galactic nuclei show rapid X-ray variability with a time scale of ~1 d. For example, the nucleus of Seyfert galaxy NGC 4151 exhibits frequent flarelike events on a time scale of days (Lawrence 1980). In addition to NGC 4151, two Seyfert galaxies NGC 3227 and MCG 5-23-16 also show variability consistent with a time scale of ~1 d (Tennant and Mushotzky 1983). The time scales of these variabilities are of the same order of the pulsation periods of accretion disks around black holes of $\sim10^8\,M_\odot$.

It is natural in the theoretical viewpoint that many accretion disks pulsate. Observations of several objects appear to support this idea. Of course, it is necessary to investigate pulsations in more realistic disks in order to compare periods of eigenmodes with observations. We expect, however, that the results in this paper are qualitatively insensitive to disk models as long as geometrically thin disks are considered.

The authors thank an anonymous referee for pointing out an error in interpreting

numerical results by the WKBJ method and for drawing their attention to the asymptotic theory of stellar nonradial pulsations. Numerical computations were performed at the Data Processing Center of Kyoto University.

Appendix. The Relativistic Epicyclic Frequency

To derive the relativistic epicyclic frequency κ observed at infinity, we consider particle orbits in the equatorial plane of the Kerr metric. Units with $G=1=c$ are chosen throughout the Appendix. Greek indices refer to four coordinates. In Boyer–Lindquist coordinates, the metric in and near the equatorial plane is (Novikov and Thorne 1973)

$$ds^2=-\frac{r^2\Delta}{A}dt^2+\frac{A}{r^2}(d\phi-\omega dt)^2+\frac{r^2}{\Delta}dr^2+dz^2\,, \tag{A1}$$

or in contravariant form

$$\left(\frac{\partial}{\partial s}\right)^2=-\frac{A}{r^2\Delta}\left(\frac{\partial}{\partial t}\right)^2-\frac{2A\omega}{r^2\Delta}\left(\frac{\partial}{\partial t}\right)\left(\frac{\partial}{\partial\phi}\right)+\frac{\Delta}{r^2}\left(\frac{\partial}{\partial r}\right)^2$$
$$+\frac{r-2M}{r\Delta}\left(\frac{\partial}{\partial\phi}\right)^2+\left(\frac{\partial}{\partial z}\right)^2. \tag{A2}$$

Here functions Δ, A, and ω are defined by

$$\Delta=r^2-2Mr+a^2\,, \tag{A3}$$

$$A=r^4+r^2a^2+2Mra^2\,, \tag{A4}$$

$$\omega=2Mar/A\,, \tag{A5}$$

where a is the angular momentum per unit mass of the Kerr black hole ($0\leqq a\leqq M$).

The energy-momentum tensor of a particle of unit mass is

$$T^{\mu\nu}=u^\mu u^\nu\,, \tag{A6}$$

where u^μ is the particle's 4-velocity dx^μ/ds. Then, the Euler equation is

$$u^\mu{}_{;\nu}u^\nu=0\,. \tag{A7}$$

We first consider a circular motion in the equatorial plane. Then it follows from equation (A7) that the angular velocity of a circular motion observed at infinity is

$$\tilde{\Omega}\equiv\frac{d\phi}{dt}=\pm\frac{M^{1/2}}{r^{3/2}\pm aM^{1/2}}\,. \tag{A8}$$

In this and all subsequent formulae, the upper sign refers to direct orbits, while the lower one refers to retrograde ones. The redshift factor u^t at the radius of the circular orbit, which we denote by U^t, is then

$$U^t=\frac{r^{3/2}\pm aM^{1/2}}{r^{3/4}(r^{3/2}-3Mr^{1/2}\pm 2aM^{1/2})^{1/2}}\,. \tag{A9}$$

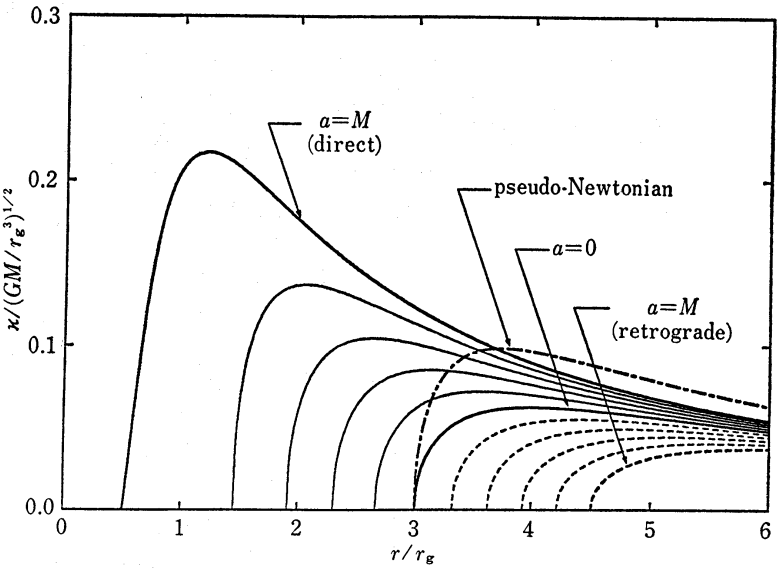

Fig. A1. The functional form of the epicyclic frequency $\kappa(r)$ observed at infinity for various values of the hole's specific angular momentum a. Solid curves are for direct orbits and broken curves for retrograde ones. Values of a of two adjacent curves differ by $0.2M$; from the left, they decrease from M to 0 for solid curves and increase from $0.2M$ to M for broken ones. For comparison, $\kappa(r)$ in the pseudo-Newtonian case is indicated by the dash-dotted curve.

Now, we consider a perturbed motion in the equatorial plane, i.e., a motion infinitesimally deviated from the circular one. The coordinate velocity is written as

$$\frac{dx^\mu}{dt}=(1, v^r, \tilde{\Omega}+v^\phi, 0)\,. \tag{A10}$$

Here v^r and v^ϕ denote the infinitesimal velocity associated with the perturbation. To derive linearized equations for v^r and v^ϕ, it is convenient to rewrite the Euler equation (A7) into the form

$$\left[\left(\frac{dx^\mu}{dt}\right)_{;\nu}+\frac{dx^\mu}{dt}\frac{\partial}{\partial x^\nu}\ln u^t\right]\frac{dx^\nu}{dt}=0\,. \tag{A11}$$

Here, u^t is expressed as

$$u^t=U^t\left[1+(U^t)^2\frac{A}{r^2}(\tilde{\Omega}-\omega)v^\phi\right], \tag{A12}$$

which is a linearized form of equation (A1).

Substituting equations (A10) and (A12) into equation (A11), we finally obtain linearized equations for v^r and v^ϕ:

$$\frac{\partial v^r}{\partial t}\mp 2\Delta M^{1/2}r^{-5/2}v^\phi=0, \tag{A13}$$

$$\frac{\partial v^\phi}{\partial t}\pm\left[\frac{M^{1/2}r^{1/2}(r^2-6Mr\pm 8aM^{1/2}r^{1/2}-3a^2)}{2\Delta(r^{3/2}\pm aM^{1/2})^2}\right]v^r=0\,. \tag{A14}$$

The epicyclic frequency κ is immediately derived from these equations:

$$\left(\frac{\partial^2}{\partial t^2}+\kappa^2\right)\begin{pmatrix} v^r \\ v^\phi \end{pmatrix}=0\,, \tag{A15}$$

where

$$\kappa^2=\frac{M(r^2-6Mr\pm 8aM^{1/2}r^{1/2}-3a^2)}{r^2(r^{3/2}\pm aM^{1/2})^2}\,. \tag{A16}$$

The functional form of $\kappa(r)$ is shown in figure A1 for various values of a. For comparison, $\kappa(r)$ in the pseudo-Newtonian case is also shown.

References

Blumenthal, G. R., Yang, L. T., and Lin, D. N. C. 1984, *Astrophys. J.*, **287**, 774.

Carroll, B. W., Cabot, W., McDermott, P. N., Savedoff, M. P., and Van Horn, H. M. 1985, *Astrophys. J.*, **296**, 529.

Cox, J. P. 1981, *Astrophys. J.*, **247**, 1070.

Cox, J. P., and Everson, B. L. 1983, *Astrophys. J. Suppl.*, **52**, 451.

Kato, S. 1978, *Monthly Notices Roy. Astron. Soc.*, **185**, 629.

Kato, S. 1979, *Publ. Astron. Soc. Japan*, **31**, 495.

Kato, S. 1983, *Publ. Astron. Soc. Japan*, **35**, 249.

Kato, S., and Fukue, J. 1980, *Publ. Astron. Soc. Japan*, **32**, 377.

Lawrence, A. 1980, *Monthly Notices Roy. Astron. Soc.*, **192**, 83.

Liang, E. P., and Nolan, P. L. 1984, *Space Sci. Rev.*, **38**, 353.

Livio, M., and Shaviv, G. 1981, *Astrophys. J.*, **244**, 290.

Meekins, J. F., Wood, K. S., Hedler, R. L., Byram, E. T., Yentis, D. J., Chubb, T. A., and Friedman, H. 1984, *Astrophys. J.*, **278**, 288.

Novikov, I. D., and Thorne, K. S. 1973, in *Black Holes*, ed. C. DeWitt and B. S. DeWitt (Gordon and Breach, New York), p. 343.

Okazaki, A. T., and Kato, S. 1985, *Publ. Astron. Soc. Japan*, **37**, 683.

Paczyński, B., and Wiita, P. J. 1980, *Astron. Astrophys.*, **88**, 23.

Shibahashi, H. 1979, *Publ. Astron. Soc. Japan*, **31**, 87.

Tennant, A. F., and Mushotzky, R. F. 1983, *Astrophys. J.*, **264**, 92.

Unno, W., Osaki, Y., Ando, H., and Shibahashi, H. 1979, in *Nonradial Oscillations of Stars* (University of Tokyo Press, Tokyo), p. 100.

Van Horn, H. M., Wesemael, F., and Winget, D. E. 1980, *Astrophys. J. Letters*, **235**, L143.